Report on the results of project K 106191

„Role of retinoids in the maintenance and function of the brain barriers”

financed by National Research, Development and Innovation Office (NKFIH)

I. Immunhistological identification of RA-producing cells in barrier structures

Immunocytochemical staining for retinaldehyde dehydrogenases (Raldhs), the key enzymes of retinoic acid formation, revealed significant capacity for retinoid production in the cranial meninges in choroid plexus and in the parenchymal microvessels (Fig. 1) known to serve as mechanical and chemical barriers between the blood and the extracellular space of the brain tissue. In double immunostaining, GFAP and Raldh2 did not show co-localization indicating that astrocytes are not the main sources of local retinoic acid production.

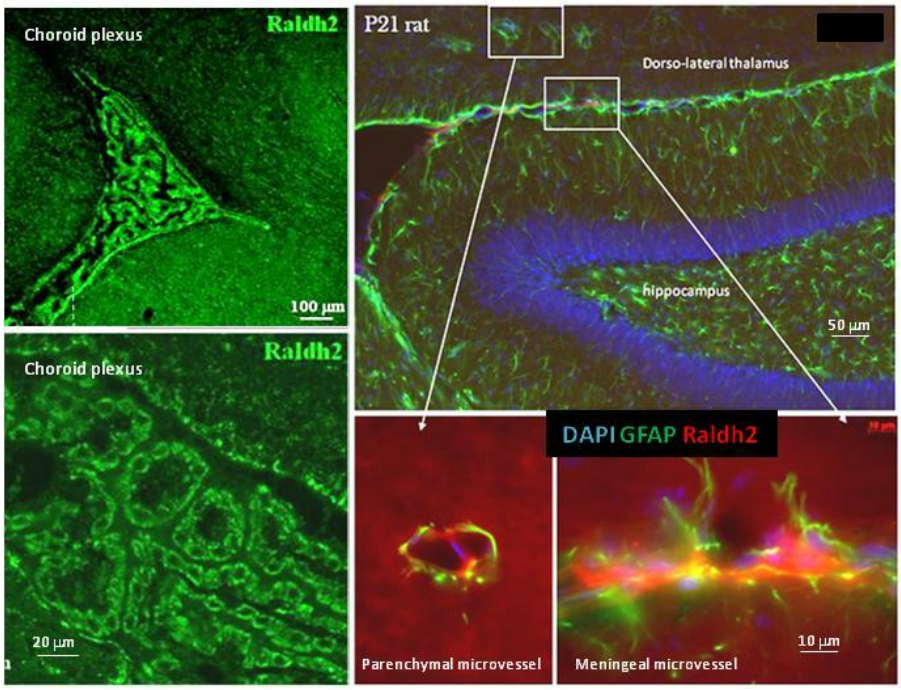

Fig.1. Immunocytochemical detection of Raldh2 enzyme in choroid plexi and around meningeal and parenchymal microvessels

More thorough investigations, however demonstrated stronger presence of Raldh2 protein in meningeal cells around the meningeal capillaries (Fig.2) indicating that meningeal cells have higher capacity to produce retinoic acid. Raldh2 staining in parenchymal microvessels (Fig.1) suggested that parenchymal endothelial cells might also provide retinoic acid.

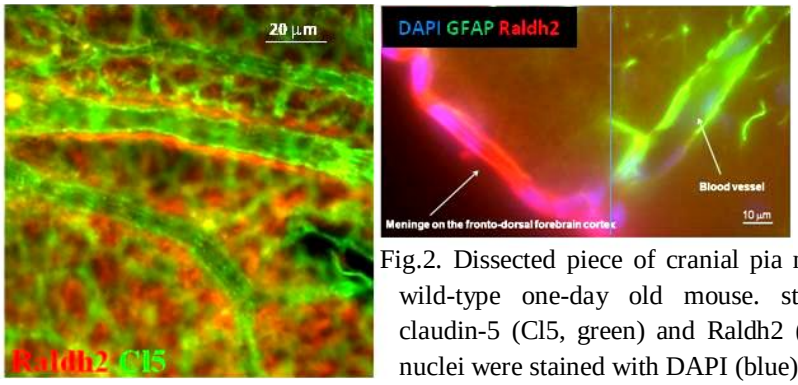

Fig.2. Dissected piece of cranial pia mater of a wild-type one-day old mouse. stained for claudin-5 (Cl5, green) and Raldh2 (red). Cell nuclei were stained with DAPI (blue).

II. Gene expression studies on dissected cranial pia mater, plexus choroideus, isolated microvessels and cellular constituents of the blood-brain barrier

Gene expression studies on isolated meninges, brain microvessel endothel cells and astrocytes verified the immuncytochemical findings, but also indicated that through the expression of other Raldh isoforms, endothelial cells might also contribute to local retinonid production.

Pia mater was removed from the dorsal forebrain surface of newborn or early postnatal (P0-P3) mice and were either rapidly fixed with paraformaldehide, or were digested with trypsin in order to isolate associated cells. Transgenic animals with constitutive (heterozigous) expression of a C3XCR1-GFP construct (Jung et al., 2000) were used to separate microglia cells and animals expressing GFP from a human GFAP promoter (Nolte et al., 2001) were used to isolate astrocytes by FACS. Pieces of choroid plexus, cortex tissue and hyppocampus were dissected and micro- and macro-vessels were isolated from homogenates of the brain tissue (Tontsch and Bauer 1989). Brain microvessel endothelial cells were prepared and cultivated according to Deli et al., (1994). Astrocytes and microglia cells were separated and cultivated according to Környei et al., (2000) and Dénes et al., (2008), respectively, or were freshly FACS-isolated from digested transgenic brain tissues or meninges.

Total RNA fractons were prepared from dissected material, isolated blood vessels and from cultivated or FACS-sorted cells. The samples were proceeded for RT-PCR studies on expression of genes coding key proteins of retinoid metabolism (Fig.3).

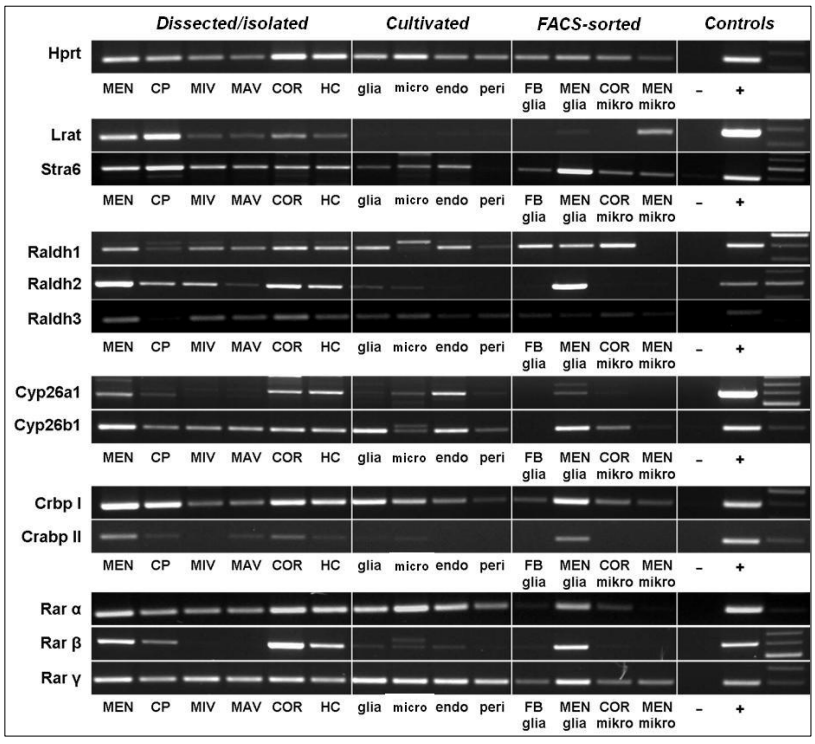

Fig.3. Expression of key components of retinoid-metabolism in different tissue samples (MEN: forebrain pia mater; CP: choroid plexus; MIV: microvessels; MAV: macrovessels; COR: cerebral cortex; HC: hippocampus) and cells (glia: astrocytes; micro: microglial cells; peri: pericytes) isolated from young postnatal mouse brain.

Genes:

Hprt: Hypoxanthine-guanine phosphoribosyl-transferase;
Lrat: lethicin:retinol acyl-transferase;
Stra6: membrane receptor for RBP;
Raldhs: retinaldehyde dehydrogenases;
Cyp26a1,b1: retinoic acid degrading enzymes;
Crbp I:cellular retinol binding protein I;
Crabp II: cellular retinoic acid binding protein II;
Rarα,β,γ: nuclear retinoic acid receptors

III. retinoid content in mouse brain meninges, choroid plexus, and liquor

After mapping the potential retinoid production by gene expression analysis, the retinoid content of the structures was investigated by HPLC-MS-MS analyses.

Cerebrospinal fluid (CSF) was sampled from the *cisterna magna* of deeply anesthetized adult CD1 and C57bl mice under stereo-microscope with gentle suction through a glass microcapillary. After liquor collection, mice were transcardially perfused with PBS. The brains were removed and the choroid plexi were dissected from the lateral ventricles and from ventricle IV. The pia mater was removed from the brain surface with special care on not to contaminate the meningeal samples with parenchymal tissue. Dura mater was scraped out from the cranium. The solid samples were washed with PBS, and were frozen and stored at −80°C until required. All tissues were dissected under yellow light to prevent light-induced break-down of retinoids. Individual samples were pooled (*n* = 10-20 animals per sample). The samples were analyzed by Dr Ralph Rühl (Lab. Nutritional Bioactivation and Bioanalysis, Dept. Biochemistry and Molecular Biology, Univ. Debrecen). as it was described earlier (Környei et al., 2007; Rühl, 2006).

HPLC-MS-MS analysis confirmed the presence of *all-trans* retinoic acid (RA) in the major barrier structures of the mouse CNS (Table 1). The highest RA concentrations were found in the dura mater, while the retinol level was the highest in the choroid plexus. Two novel, bioactive retinoids, (9C-NEW and AT-NEW; R. Rühl et al; 2015.) were found in high concentrations in the meninges and also in the choroid plexus. Retinoic acid presumably released from these sources was found in the cerebrospinal fluid, in 0.3-1 nM concentration (Table 2). HPLC-MS-MS analyses indicated some strain-dependent differences in the distribution of retinoids (table 1 and 2). While a*ll-trans* retinoic acid and retinol was detected in all major CNS barrier structures of both CD1 and C57bl mouse strains, the amount of retinoids in pia mater, dura mater and choroid plexus showed important alterations suggesting strain-dependent variations in the intracerebral production-sites of active retinoids.

Table 1. Retinoid content in the brain meninges and choroid plexus of CD1 and C57bl mice

Retinoid derivatives	Concentration of retinoids [ng/g]					
	PIA MATER		**CHOROID PLEXUS**		**DURA MATER**	
	CD1	C57bl	CD1	C57bl	CD1	C57bl
ATRA	0.2	0.5	0.5	0.4	3.3	1.3
ROL	13.1	23.0	54.5	29.9	21.7	13.7
*9C-new	4.4	5.3	7.5	2.6	17.5	7.0
*AT-new	44.4	13.7	18.2	8.6	17.5	11.3
number of mice	*20*	*24*	*20*	*24*	*20*	*24*
Tissue weight total	48 mg	43 mg	44 mg	84 mg	12 mg	30 mg

Table 2. Retinoid concentrations in the cerebro-spinal fluid and hippocampus of CD1 and C57bl mice

Retinoid derivatives	Concentration of retinoids [ng/ml]							
	LIQUOR				**HIPPOCAMPUS**			
	CD1 mice		C57bl mice		CD1 mice		C57bl mice	
ATRA	0,3	0,1	0,6	0,5	0,5	2,1	1,9	2,5
ROL	1,7	1,4	2,0	0,9	6,8	19,2	22,2	14,0
9C-new	7,9	2,4	7,0	9,8	2,0	9,2	5,1	3,4
AT-new	2,6	1,4	4,6	6,0	6,7	50,6	36,0	78,4
number of mice	*10*	*10*	*11*	*13*	*10*	*10*	*11*	*13*
Tissue volume total	70 ul	70 ul	50 ul	55 ul	130 mg	108 mg	100 mg	110 mg

IV. Content and effects of retinoic acid in cultivated brain tissue cells

HPLC/MS studies demonstrated that cultured mouse astrocytes, neural stem cells, brain endothelial cells and in microglial cells contain varying quantities of both retinol and RA (Orsolits et al; 2013). Retinoids are known to induce severe changes in cellular phenotypes mainly due to regulation of gene expression through nuclear retinoid receptors. The different cells, however, displayed different reactions in response to loading with external RA.

Brain microvessel endothelial cells prepared from adult (P59) mice and maintained for 9 days in vitro were treated with 100 nM all-trans retinoic acid or with 100 nM AGN193109 (Allergan Inc., Irvine, CA, USA), a potent inhibitor of nuclear retinoid receptors. After a 2-hour inhibition of nuclear retinoid receptors, Claudin-5 was reduced in the cell membranes and accumulated in the cytoplasm (Fig.4) indicating damages in cell to-cell contacts and suggesting the importance of RA in maintaining the „normal" struture of brain microvessel-derived endothelial cells.

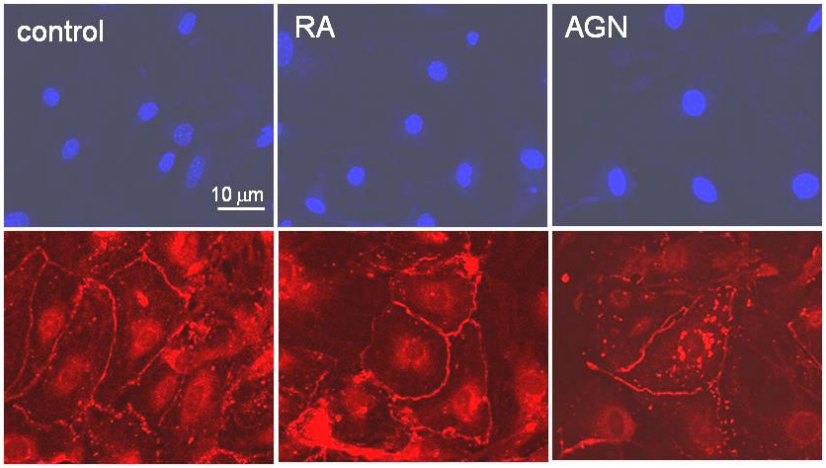

Fig.4. Morphological changes of brain microvessel endothelial cells in response to a 2-hour presence of 100 nM all-trans retinoic acid (RA) or 100 nM AGN193109 nuclear retinoic acid receptor-blocker. The cultures were stained with anti-Claudin5 antibodies (red; lower panels), and cell nuclei were visualized by DAPI (blue; upper panel).

NE-4C embryonic neural stem cells differentiate into neurons in response to treatment with RA (Schlett, Madarasz 1997) Measuring the O2-consumption and proton release of cells (Seahorse Cell Analyzer FX), important changes were found between the non-induced stem cells and the ATRA-induced progenies (Fig.5) (Jády et al.; 2016).

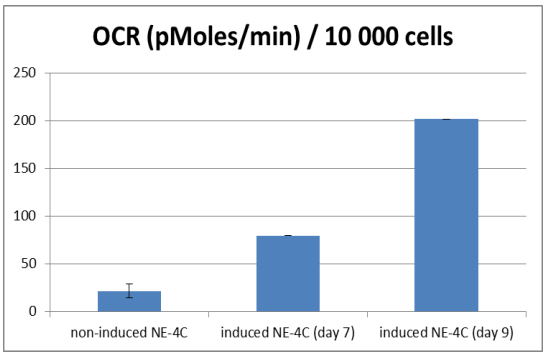

Fig.5. O_2-consumption by NE-4C stem cells and RA induced NE-4C-progenies (OCR: oxygen consumption rate)

Non-induced and RA-induced cells gave different metabolic responses to starvation, or to supplementation of starvation medium with single metabolic fuel molecules. Despite of

enhanced O2-consumption, induced cells did not increase mitochondrial O2 uptake in response to lactate or pyruvate, known to enhance oxidative phosphorylation and increasing O2 consumption by non-induced cells (Fig. 6).

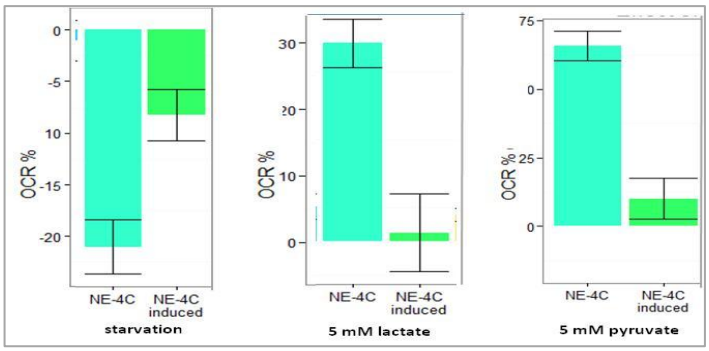

Fig.6. Changes in O_2-consumption of NE-4C stem cells and RA induced NE-4C-progenies in comparison to values in „non-starving" values (OCR: oxygen consumption rate;)

In search for reasons behind the highly different metabolic responses, the expression of several metabolic key proteins were compared by qPCR technique. Important differences were found in the expression of glucose transporters, the key regulatory kinase of pyruvate dehydrogenase (*pdk4*) and in the transcription of the pentose-phosphate pathway regulating phosphofructo-kinase 3 enzyme (*pfk3*) (Fig 7).

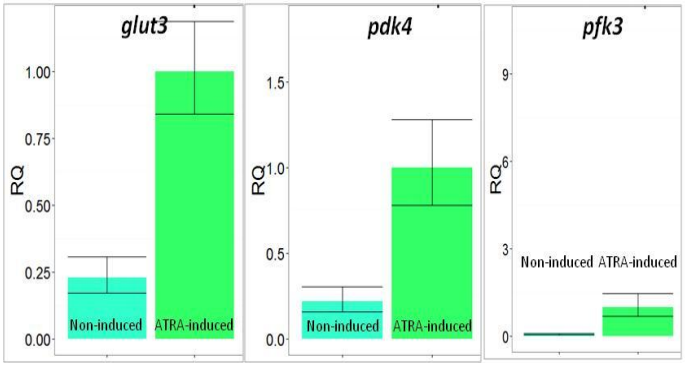

Fig. 7. Relative transcription rate (RG related to *hprt* housekeeping gene) of glucose transporter3 (*glut3*), pyruvate dehydrogenase-kinase (*pdk4*) and phosphofructo-kinase 3 (*pfk3*) in non-induced NE-4C stem cells and in RA-induced NE-4C derivatives.

The data indicate fundamental reorganization of the metabolic pathways in response to RA-induction. As RA induces neuronal differentiation in NE-4C cells, the observed reorganization might be due either to the RA-induced formation of the neuronal phenotype or to direct genom-level metabolic effects of RA. In both cases, the presence of RA can severely influence the metabolism of cells, at least some differentiation-capable neural cells.

V. Models for studying physiological barrier functions

Short-term and long-term body distribution of 50 nm fluorescent polystyrene nanoparticles (PS NPs) with carboxylated (PS-COOH) or PEGylated (PS_PEG) surfaces were investigated

after a single **(**2.1µg particle mass /g bodyweight) intravenous injection into adult male and pregnant mice. Mice were sacrificed 5 minutes and 4 days after the injection by overdose anaesthetics. 60µm vibratome sections were made from different organs**.**

The size of NPs prevented the rapid renal clearing known to retain protein-complexes with size of about 10 nm. The penetration of particles through the blood-brain barrier and placenta was investigated by confocal microscopic fluorescence spectrum analysis in order

to distinguish NP-emitted fluorescent light from background fluorescene of living cells and tissues (Kenesei et al., 2016)

The spectrum of the light emitted by NPs was recorded in different environments including MilliQ water, physiological buffers, cell culture media, as well as on the surface of fixed and fresh tissue sections. Fluorescence spectra of NPs were used as positive control, while the autofluorescence-spectrum of the biological specimen served as negative control (Fig.8). For spectral evaluation 457nm argon ion laser was used as excitation source, and the emitted light was detected by the spectral detector unit from 468nm to 548nm, with a spectral resolution of 2,5nm. In order to record continuous spectrum, a 20/80 beam splitter (BS20/80) with continuous transmission was used instead of a paired dichronic mirror arrangement.

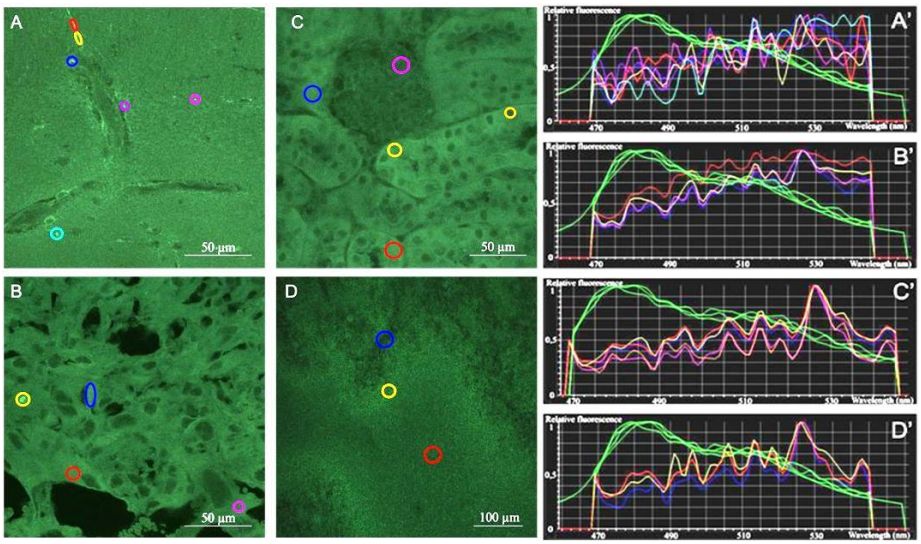

Fig.8. Microscopic autofluorescence of fixed tissue sections of mouse forebrain (A), placenta (B), kidney (C) and spleen (D). The spectra of individual regions of interest (coloured circles) are shown on the right (A', B',C', D') pictures with the same colour. The three green curves on each spectrum show the fluorescence of particles pipetted to corresponding section in distilled water, dried on the section or dried and then mounted with moviol together with section. Y axis : the relative intensity of the emitted light, X axis : the wavelength of the emitted light.

Regions of interest (ROIs) were delineated and analyzed on corresponding sections of nanoparticle-treated and non-treated organs. The photocurrent intensities detected at different wavelengths (emission spectra) were plotted and were compared to the autofluorescence spectra (negative control) and to the spectrum of nanoparticles (positive control) (Fig.8).

If excited with 457 nm wavelength illumination, FITC-labelled PS NPs emitted light with wavelengths from 470nm to 550 nm with the highest intensity between 475-485 nm. In this range, the intensity of autofluorescence of tissue sections was low allowing precise decision on the presence or absence of assembled fluorescent particles in the selected spot of sections.

In the brain, 5 minutes after the injection, many PS-COOH particles were found in the large vessels and small capillaries, while PS-PEG particles were not found (Fig.9 A, B). Inside the brain parenchyma, however, NPs were not found. Similar short-term distribution of particles was seen in the placenta: 5 minutes after the injection PEGylated particles were not found, while carboxylated particles were stuck in placental lacunas (Fig.9 C and D). Particles were not seen in any embryonic tissues indicating the proper barrier function of the placenta.

After 4 days, both PS-COOH and PS-PEG particles were completely cleared from the brain and the placenta (Kenesei et al., 2016). As a contrast, heavy particle-contamination was seen in the spleen (Fig.10) and in the liver.

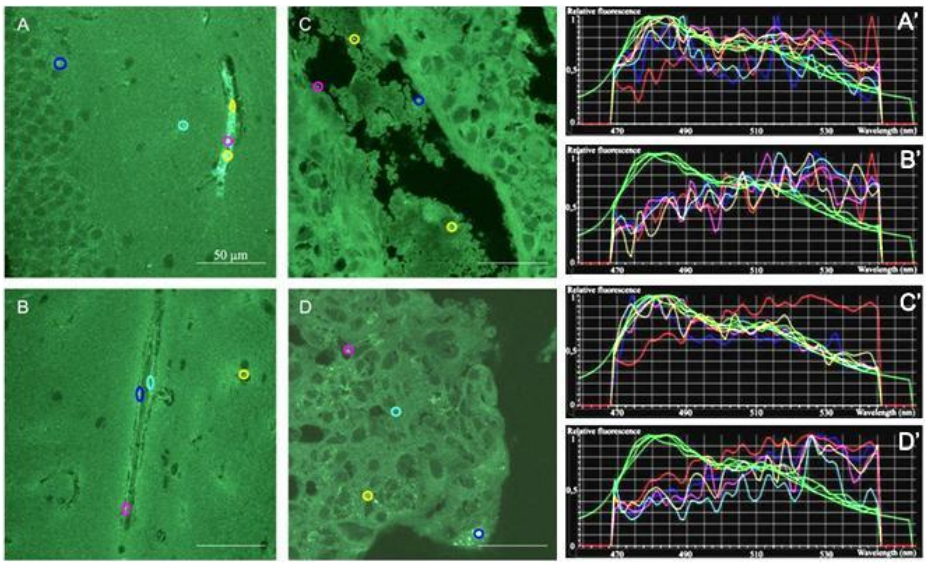

Fig.10. Five minutes after loading, different distribution of PS-COOH and PS-PEG particles was found in the adult mouse forebrain and in the placenta (day 15 post conception). (A, A': PS-COOH NPs in the forebrain; B, B': PS-PEG NPs in the forebrain; C, C': PS-COOH NPs in the placenta; D, D': PS-PEG NPs in the placenta). Coloured circles on microscopic pictures show the spectrum-analyzed regions. On graphs of spectrum analyses, spectra of individual regions are shown in the same colour. The green curves indicate the fluorescence spectra of NPs, and serve as positive controls

The data demonstrated that fluorescence spectrum analysis can serve as a method to monitor the active accumulation of labelled particles in the brain, thus can be applied to study the permeability changes of the blood-brain barrier.

References

Deli MA, Dung NTK, Joó F. 1994. Isolation and culture of endothelial cells from cortical microvessels of the rat and piglets. In: Drug transport across the blood-brain barrier (BBB). de Boer ABG and Sutanto W (eds), BIOMED-Concerted action, Leiden, pp. 175-188, 1994.

Denes, Adam, Ferenczi, Szilamer, Halasz, Jozsef, Kornyei, Zsuzsanna, Kovacs, Krisztina J. 2008. Role of CX3CR1 (fractalkine receptor) in brain damage and inflammation induced by focal cerebral ischemia in mouse. JOURNAL OF CEREBRAL BLOOD FLOW AND METABOLISM 28 **(**10**):** 1707-1721

Jády AG, Nagy ÁM, Kőhidi T, Ferenczi S, Tretter L, Madarász E. 2016. Differentiation-dependent energy production and metabolite utilization: A comparative study on neural stem cells, neurons, and astrocytes. Stem Cells Dev. 2016. 25(13):995-1005. doi: 10.1089/scd.2015.0388.

Jung S, Aliberti J, Graemmel P, Sunshine MJ, Kreutzberg GW, Sher A, Littman DR. 2000. Analysis of fractalkine receptor C3XCR1 function by targeted deletion and green fluorescent protein reporter gene insertion. Mol Cell Biol 20:4106–14

Kenesei Kata, Kumarasamy Murali, Árpád Czéh, Jordi Piella, Victor Puntes, Emília Madarász. 2016. Enhanced detection with spectral imaging fluorescence microscopy reveals tissue- and cell-type-specific compartmentalization of surface-modified polystyrene nanoparticles. J. Nanobiotechnology; 2016; 14:55-69

Környei Zs., Gócza E., Rühl R., Orsolits B., Vörös E., Szabó B., Vágovits B., Madarász E. 2007. Astroglia-derived retinoic acid is a key factor in glia-induced neurogenesis. FASEB J. 21(10):2496-509.

Murali K, Kenesei K, Li Y, Demeter K, Környei Zs, Madarász E. 2015. Uptake and bio-reactivity of polystyrene nanoparticles is affected by surface modifications, ageing and LPS adsorption: *in vitro* studies on neural tissue cells. NANOSCALE 7:(9) pp. 4199-4210. (2015);

Nolte C, Matyash M, PivnevaT, SchipkeCG, OhlemeyerC, 2001. GFAP promoter-controlled EGFP-expressing transgenic mice: a tool to visualize astrocytes and astrogliosis in living brain tissue. Glia 33: 72-86.

Orsolits B., Borsy A., Madarász E., Mészáros Zs., Kőhidi T., Markó K., Jelitai M, Welker E., Környei Zs. 2013. Retinoid machinery of distinct neural stem cell populations with different retinoid responsiveness. Stem Cells Devl. 2013;22(20):2777-93

Rühl R, Krzyżosiak A, Niewiadomska-Cimicka A, Rochel N, Szeles L, Vaz B, Wietrzych-Schindler M, Álvarez S, Szklenar M, Nagy L, de Lera AR, Krężel W., 2015. 9-cis-13,14-Dihydroretinoic Acid Is an Endogenous Retinoid Acting as RXR Ligand in Mice. PLoS Genet. 2015 Jun 1;11(6):e1005213)

Rühl, R. 2006. Method to determine 4-oxo-retinoic acids, retinoic acids and retinol in serum and cell extracts by liquid chromatography/diode-array detection atmospheric pressure chemical ionisation tandem mass spectrometry. Rapid Commun. Mass. Spectrom. 20:2497–2504

Schlett K., Madarasz E., 1997. Retinoic acid induced neural differentiation in a neuroectodermal cell line immortalized by p53 deficiency. J Neurosci Res. 47: 405-415 .

Tontsch U and Bauer HC. 1989. Isolation, characterization and long-term cultivation of porcine and murine cerebral capillary endothelial cells. Microvasc. Res. **37**:148-161.

***Full-length publications on the project results*:**

Emília Madarász (2013). Diversity of Neural Stem/Progenitor Populations: Varieties by Age, and Regional Origin and Environment, Neural Stem Cells - New Perspectives, Dr. Luca Bonfanti (Ed.), ISBN: 978-953-51-1069-9, InTech,

Orsolits B., Borsy A., Madarász E., Mészáros Zs., Kőhidi T., Markó K., Jelitai M, Welker E., Környei Zs. Retinoid machinery of distinct neural stem cell populations with different retinoid responsiveness. Stem Cells Devl. 2013. 22(20):2777-93 IF: 4.459

Szilvia Veszelka, Andrea E Tóth, Fruzsina R Walter, Zsolt Datki, Emese Mózes, Lívia Fülöp, Zsolt Bozsó, Eva Hellinge, Monika Vastag, Barbara Orsolits, Zsuzsanna Környei, Botond Penke, Mária A Deli Docosahexaenoic Acid Reduces Amyloid-B Induced Toxicity in Cells of the Neurovascular Unit Journal of Alzheimer's disease; 2014. DOI:10.3233/JAD-120163. IF: 3,74

Beáta Hegyi, Zsuzsanna Környei, Szilamér Ferenczi, Rebeka Fekete, Gyöngyi Kudlik, Krisztina J. Kovács, Emília Madarász, Ferenc Uher. Regulation of mouse microglia activation and effector functions by bone marrow-derived mesenchymal stem cells. Stem Cells Devl. 2014. 1;23(21):2600-12 IF: 4.459

Murali K, Kenesei K, Li Y, Demeter K, Környei Zs, Madarász E. Uptake and bio-reactivity of polystyrene nanoparticles is affected by surface modifications, ageing and LPS adsorption: *in vitro* studies on neural tissue cells. NANOSCALE 7:(9) pp. 4199-4210. (2015); IF: 7,997

Jády AG, Nagy ÁM, Kőhidi T, Ferenczi S, Tretter L, Madarász E. Differentiation-dependent energy production and metabolite utilization: A comparative study on neural stem cells, neurons, and astrocytes. Stem Cells Dev. 2016. 25(13):995-1005. doi: 10.1089/scd.2015.0388. IF: 3,77

Kata Kenesei, Kumarasamy Murali, Árpád Czéh, Jordi Piella, Victor Puntes, Emília Madarász. Enhanced detection with spectral imaging fluorescence microscopy reveals tissue- and cell-type-specific compartmentalization of surface-modified polystyrene nanoparticles. J. Nanobiotechnology; 2016; 14:55-69 IF: 4,27